Research on the response model of microbolometer*

Sui Xiu-Bao(隋修宝)†, Chen Qian(陈 钱), Gu Guo-Hua(顾国华) and Liu Ning(刘 宁)

School of Electronic Engineering and Optoelectronic Technology, Nanjing University of Science and Technology, Nanjing 210094, *China*

(Received 24 February 2010; revised manuscript received 22 March 2010)

There are certain limitations in the application of uncooled focal plane array (FPA) detector due to the lack of an effective response model which reliably transforms the target temperature to analog output voltage. This paper establishes the response model of microbolometer through researching the detection theory of microbolometer and the heat balance equation under the condition of the pulsed voltage bias. In the establishing process, we simplified the heat balance equation to acquire a simple answer. The experimental data show that, in the temperature dynamic range of 30 K, the biggest tolerance between the model data and the experiment data is 0.2 K; while in the temperature dynamic range of 100 K, it is 1 K. This model can reflect the real response of the microbolometer with only small differences which are acceptable in engineering applications.

Keywords: microbolometer, detection theory, response model, capacitive transimpedance amplifier

PACC: 8732L, 7820J, 4440, 4280Q

1. Introduction

In recent decades, microbolometer has played an important role in many fields, such as, (i) in the national security equipments; (ii) in the high-tech local wars; and (iii) in the civil systems.[1,2] Despite the wide applications listed above, however, the employment of microbolometer is hampered by the lack of a model which transforms the targets temperature to the analog output of FPA. In the large-scale applications, microbolometer is largely working as a component implemented in a system, thus a mathematical model which can be used to calculate the relationship between the input and output signals is due to appearing in order to make easier the assessment of the system resources as well as the system design. Accordingly, the model of microbolometer has received much attention. For example, noise equivalent power model of the microbolometer was put forward in Ref. [3], R–T model of the microbolometer was proposed in Ref. [4], response rate model of microbolometer was proposed in Ref. [5], and the relation model of target irradiation power and thermistor temperature was proposed in Ref. [6]. However, there are so many parameters involved in the model of microbolometer, such as the integration time, TCR (temperature coefficient of resistance), integration capacitance, and frame time, and so on, it is hard to calculate the whole mathematical model precisely, which means that the models mentioned above are incomprehensive and can only offer limited help.

In the engineering applications, the establishment of any model has to be based on the theory of the device being concentrated; meanwhile, the complete precise mathematical solution is not seriously required. A reasonable approximation is very effective in the acceptable tolerance range.[7] This paper deeply researches the imaging theory of the resistance-type microbolometer and introduces a complete model of it, and verifies its practicality to microbolometer according to the experimental data.

2. Detection theory of microbolometer

The sensitive element of the resistance-type microbolometer consists of thermistors. The basic principle is: when the outside IR radiation injects on the thermistors, the temperature of these thermistors starts to change, the resistance value is also changed with the temperature, so that the change of the resis-

*Project supported by the National Defense Pre-research Fund of China (Grant No. 50405050303), the Natural Science Foundation of Jiangsu Province of China (Grant No. BK2009049).

†Corresponding author. E-mail: sxbhandsome@163.com

© 2010 Chinese Physical Society and IOP Publishing Ltd

tance value can be transformed to the change of the output voltage by proper readout circuit, which can achieve the aim of detecting the IR radiation.[8−11] Figure 1(a) is the typical structure schematic diagram of the resistance-type microbolometer which is placed in the vacuum device in order to prevent the effect of thermal convection on the sensitive element from the surrounding environment. The IR sensitive elements are fixed above the substrate by the supporting foot bridge; this bridge plays roles of mechanical support and the path of the thermal conduction and the electronics conduction, so the only two ways of exchanging heat between the surrounding environment and the pixel are the thermal conduction through the bridge and the radiation. The output signal generated by the pixel of microbolometer must depend on the bias voltage, that is to say, by supplying certain voltage on the pixel of the microbolometer, the bias current can be generated to measure the radiation temperature. Once the bias voltage has been applied to the pixel, the electro-thermal effect is bond to happen. The electro-thermal power generated by the bias voltage is much bigger than the IR radiation power received by the sensitive element, the fast growing heat in microbolometer can greatly increase the temperature of the sensitive element, and which may probably update the temperature dynamic range of the signal into an unacceptable level. Meanwhile, the noise of the microbolometer is due to increase under the high bias voltage. So, the microbolometers in the market usually use the pulsed voltage bias to ensure either the readout of the valid signal or the pixel temperature at a low level. The main thermal exchanging way of microbolometer is shown in Fig. 1(b), so the heat balance equation of the microbolometer during the bias period of the pixel is:

$$C\frac{\mathrm{d}T}{\mathrm{d}t} = \frac{V_\mathrm{b}^2}{R(T)} + \varepsilon_\mathrm{e}P_\mathrm{t} + \varepsilon_\mathrm{e}P_\mathrm{s} - (2A)\varepsilon_\mathrm{e}\sigma T^4 - G_\mathrm{leg}(T - T_\mathrm{s}), \quad (1)$$

where C represents the heat capacitance of the sensitive element; T represents the temperature of the sensitive element; G represents the thermal conductivity of the supporting bridge; T_s represents the substrate temperature; ε_e represents the emissivity; P_t represents the IR radiation power which injects on the sensitive element through the IR optical system; P_s represents the IR power that radiates to the sensitive element from the substrate, of which the detailed expression is: $P_\mathrm{s} = A_\mathrm{s}\sigma T_\mathrm{s}^4$; A_s represents the area of the substrate; A represents the surface area of the pixel of microbolometer; σ represents the Stefan–Boltzmann constant. The sensitive element of microbolometer is a thin lamella of which the radiation area is almost double the upper surface of the pixel, and that in Eq. (1), the IR power radiated from the pixel of microbolometer is approximately described as $(2A)\varepsilon_\mathrm{e}\sigma T^4$ without causing any error; V_b represents the bias voltage applied to the pixel of microbolometer; $R(T)$ represents the resistance of the sensitive element of microbolometer.

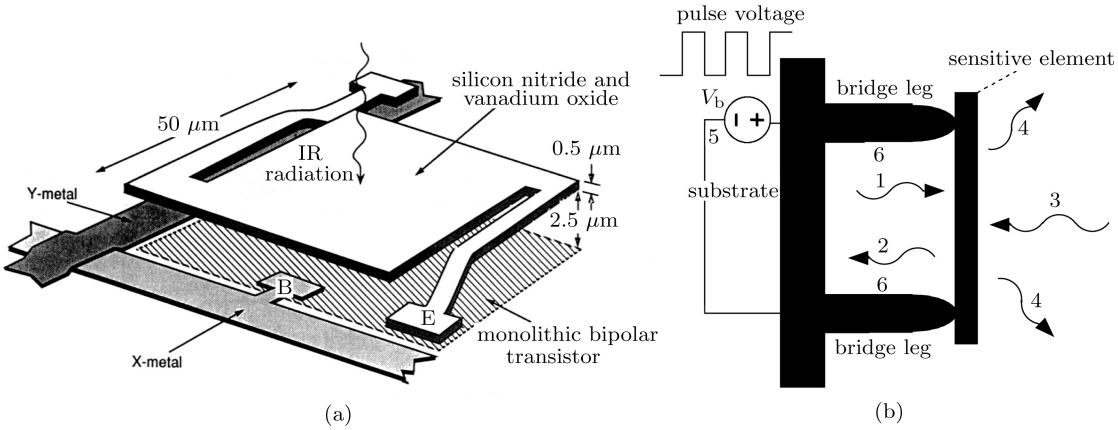


Fig. 1. Schematic diagram of microbolometer. (a) Structure scheme of the pixel and (b) heat exchange diagram of the pixel. The numbers 1–6 mean that 1: represents the radiation from substrate to sensitive element; 2: the radiation from sensitive element to substrate, 3: the radiation from the targets to sensitive element, 4: radiation from sensitive element to surrounding environment, 5: the electro-thermal power generated by the bias voltage, 6: the thermal conduction power from sensitive element to substrate though bridge legs.

3. Response mode of microbolometer

3.1. Simplification of electro-thermal power equation

The electro-thermal power equation of microbolometer is:[12,13]

$$P_{\rm v}(T) = V_{\rm b}^2/R(T) = V_{\rm b}^2/\{R(T_{\rm s})\exp[\alpha(T-T_{\rm s})]\}, \quad (2)$$

where $R(T_{\rm s})$ is the value of the thermistor at temperature $T_{\rm s}$. Considering a calculation example, the parameters are shown in Table 1. According to the parameters, the pixel temperature of microbolometer is growing fast during the pulsed voltage bias period, however, the 50-μs biasing time limits the increasing of the temperature, figure 2 shows the thermal response curve in one pulse of bias period. In the period of $(0, t_{\rm int})$, the pixel temperature curve increases almost as a straight line, so the electro-thermal power can be considered as a straight line during the integration time, the gain can be defined as:

$$P_{\rm v}(T)'|_{T=T_{\rm s}} = -(V_{\rm b}^2/R(T_{\rm s}))\alpha\exp[\alpha(T-T_{\rm s})]|_{T=T_{\rm s}} = -\alpha V_{\rm b}^2/R(T_{\rm s}). \quad (3)$$

Table 1. Calculating parameters of microbolometer.

parameter	value	parameter	value
$R(T_{\rm s})$	20/kΩ	$T_{\rm s}$	300/K
$V_{\rm b}$	1/V	C	4×10^{-9}/J$\cdot$K^{-1}
$t_{\rm int}$	50/μs	$G_{\rm leg}$	10^{-7}/W$\cdot$K^{-1}
$t_{\rm f}$	30/ms	α	-0.025

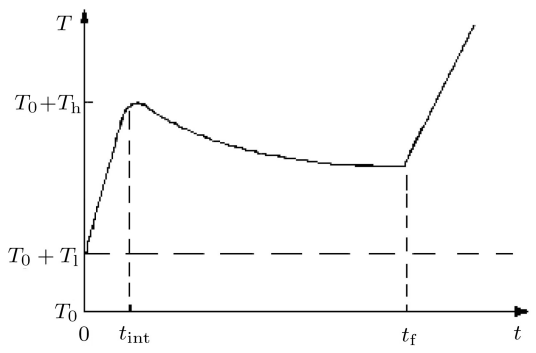


Fig. 2. Pixels temperature response during the working time of pulse bias voltage.

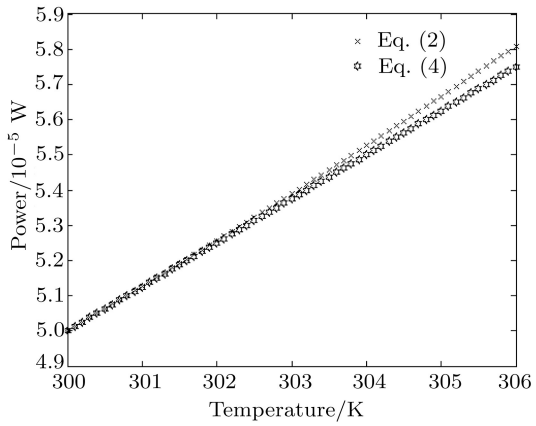


Fig. 3. Curve contrast of electro-thermal power of microbolometer sensitive element along with its temperature.

The approximate curve is:

$$P_{\rm v}(T) = k_{p_{\rm v}}T + b_{p_{\rm v}}, \quad (4)$$

where

$$k_{p_{\rm v}} = -[V_{\rm b}^2/R(T_{\rm s})]\alpha. \quad (5)$$

When $T = T_{\rm s}$, combining Eqs. (2), (4) and (5) we can obtain

$$b_{p_{\rm v}} = [V_{\rm b}^2/R(T_{\rm s})](1+\alpha T_{\rm s}). \quad (6)$$

Employing the parameters in Table 1, the curves expressed in Eqs. (2) and (4) are shown in Fig. 3. From Ref. [14], we know that if the parameters are chosen as: the pitch of the pixel is 45 μm, the emissivity of the pixel is 0.8, the F# of the optical system is 0.8, the imaging wave length of the microbolometer is 8–12 μm, then when the temperature of the sensitive element has a change of 10 mK, the corresponding IR target has a change of 1 K in temperature. Thus, if the temperature dynamic range is 100 K, the biggest temperature raise of the pixel is 1 K; according to Fig. 3, when the horizontal axis is at the coordinate of 301 K, the two curves are almost the same. The data in Table 2 show that the power difference is $0.002(\times10^{-5})$ W when the temperature of the sensitive element is 301.2 K, which means that the temperature difference of the sensitive element is 0.0016 K; if the temperature dynamic range reaches 100 K, the estimated temperature tolerance of IR target is only 1.6 K, so it is reasonable that equation (2) is replaced by Eq. (4).

Table 2. The data comparison of the electro-thermal power of the sensitive element of microbolometer with the change in temperatures.

temperature/K	300	300.4	300.8	301.2
function value of Eq. (2)/W	$5(\times10^{-5})$	$5.05(\times10^{-5})$	$5.1(\times10^{-5})$	$5.15(\times10^{-5})$
function value of Eq. (4)/W	$5(\times10^{-5})$	$5.05(\times10^{-5})$	$5.101(\times10^{-5})$	$5.152(\times10^{-5})$
value of Eqs. (2)–(4)/W	$0(\times10^{-5})$	$0(\times10^{-5})$	$-0.1(\times10^{-7})$	$0.2(\times10^{-7})$

3.2. Simplification of thermal conductivity

In Eq. (1), let

$$P_{\rm rad}(T) = (2A)\varepsilon_{\rm e}\sigma T^4. \tag{7}$$

Then the radiation heat conduction $G_{\rm rad}(T)$ of microbolometer is:

$$G_{\rm rad}(T) = \frac{{\rm d}P_{\rm rad}(T)}{{\rm d}T} = \frac{{\rm d}((2A)\varepsilon_{\rm e}\sigma T^4)}{{\rm d}T} = 8A\varepsilon_{\rm e}\sigma T^3, \tag{8}$$

which is a monotonically increasing function.

Equation (7) can also be equivalent to a straight line by the same method as the analysis of electro-thermal power. Its slope $G'_{\rm rad}(T)$ equals the value when $G_{\rm rad}(T)$ is at $T = T_{\rm s} \cdot P_{\rm rad}(T)$ can be equivalent to:

$$P_{\rm rad}(T) = 8A\varepsilon_{\rm e}\sigma T_{\rm s}^3(T - T_{\rm s}) + (2A)\varepsilon_{\rm e}\sigma T_{\rm s}^4. \tag{9}$$

Supposing that the pitch of the microbolometer is 50 μm, the value of $G_{\rm leg}$ is 2×10^{-7} W/K, $\varepsilon_{\rm e} = 0.8$, the fill factor is 0.8, then the part of the data of Eq. (7) and Eq. (9) are shown in Table 3.

Table 3. The data comparison of the IR radiation power emitted by the sensitive element of microbolometer with the change in temperatures.

temperature/K	300	301	302	303
function value of Eq. (7)/W	$1.470(\times10^{-6})$	$1.493(\times10^{-6})$	$1.509(\times10^{-6})$	$1.540(\times10^{-6})$
curve Eq. (9)/W	$1.470(\times10^{-6})$	$1.493(\times10^{-6})$	$1.509(\times10^{-6})$	$1.542(\times10^{-6})$
curve Eqs. (7)–(9)/W	0	0	0	$-0.2(\times10^{-8})$

As shown in Table 3, with the temperature rise of the sensitive element, the data difference is getting bigger and bigger, however, the value in Table 3 is one order of magnitude less than that in Table 2, so that the measurement tolerance of IR target can be totally ignored when equation (7) is replaced by Eq. (9). Meanwhile, according to Eq. (1), $P_{\rm v}(T) = V_{\rm b}^2/R(T)$ and $P_{\rm rad}(T) = (2A)\varepsilon_{\rm e}\sigma T^4$ are subject to minus calculation, since the values in the equivalent Eqs. (4) and (9) are all less than the original ones, thus in the heat balance formula, the replacement will not cause additional increase in the tolerances.

3.3. The Process of establishing the model

Combining Eqs. (1), (4) and (9), the heat balance equation during the pulse bias period can be formed as:

$$C\frac{{\rm d}T}{{\rm d}t} = k_{p_{\rm v}}T + b_{p_{\rm v}} + P_{\rm cons} + \varepsilon_{\rm e}P_{\rm t} - G(T - T_{\rm s}), \tag{10}$$

where $P_{\rm cons} = \varepsilon_{\rm e}P_{\rm s} - (2A)\varepsilon_{\rm e}\sigma T_{\rm s}^4$, $P_{\rm cons}$ is a constant for the same microbolometer; $P_{\rm t} = P_0\exp({\rm i}wt)$, P_0 is the modulated IR radiation power; w is the modulation frequency; $G = G_{\rm leg} + G_{\rm rad}(T_{\rm s})$.

Thus, the complete heat balance equation of microbolometer is:

$$C\frac{{\rm d}T}{{\rm d}t} = P_{\rm cons} + \varepsilon_{\rm e}P_0\exp({\rm i}wt) - G(T - T_{\rm s}), \tag{11a}$$

$$C\frac{{\rm d}T}{{\rm d}t} = k_{p_{\rm v}}T + b_{p_{\rm v}} + P_{\rm cons} + \varepsilon_{\rm e}P_0\exp({\rm i}wt) - G(T - T_{\rm s}), \tag{11b}$$

where the first formula is the heat balance equation without the pulse bias voltage, the second is the one with the pulse bias voltage. The general solution of

Eq. (11) is:

$$T(t) = \frac{P_{\rm cons} + GT_{\rm s}}{G} + \frac{\varepsilon_{\rm e} P_0}{C{\rm i}w + G}\exp({\rm i}wt) + c_1 \exp\Big(-\frac{G}{C}t\Big), \tag{12a}$$

$$T(t) = \frac{P_{\rm cons} + GT_{\rm s} + b_{p_{\rm v}}}{G - k_{p_{\rm v}}} + \frac{\varepsilon_{\rm e} P_0}{C{\rm i}w + G - k_{p_{\rm v}}}\exp({\rm i}wt) + c_1' \exp\Big(-\frac{G - k_{p_{\rm v}}}{C}t\Big), \tag{12b}$$

where c_1 and c_1' represent the general coefficients which will be solved in the next section.

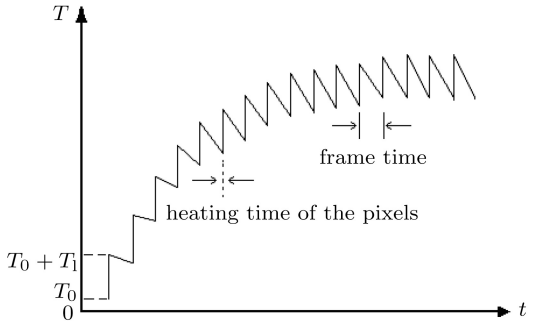


Fig. 4. Heat response curve of one sensitive element of the microbolometer under the continuous pulse bias voltage.

The heat response curve of a single sensitive element of microbolometer under the continuous pulsed bias voltage is shown in Fig. 4. Once the voltage is applied to the microbolometer, in the first pulse time, microbolometer is heated rapidly and the temperature of the sensitive element grows very fast; in the subsequent time of the frame, the temperature of the sensitive element goes down gradually until the second pulse bias comes, and then, the temperature of the pixel starts rising again on the basis of the first frame time, and decreasing when the pulse is over. Repeatedly, when the heat absorbed by the sensitive element is equal to the heat radiated from it, the temperature of the pixel will vibrate in a small interval, which means that the sensitive element reaches the thermal equilibrium. When the temperature of the sensitive element is stable, the heat response curve in one frame time can be acquired by translating other curves in other frame time along with the t axis. Supposing that the original time of using pulsed bias voltage is 0 during the temperature-stable period of the pixel, the change of the temperature range of the pixel with the time is shown in Fig. 5, where $t_{\rm int}$ is the time of the pulse voltage bias; $t_{\rm f}$ is the frame time. Curve a is the response curve without thepulse bias voltage; b is the one with the pulse bias voltage; c is the one without the pulse bias voltage in the next frame. According to Eq. (12), three equations of these curves can be formulated as:

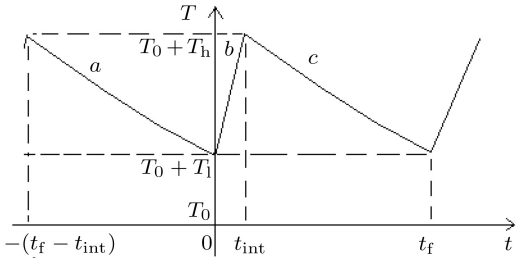


Fig. 5. Heat response curve of the pixel of microbolometer in quasi-steady-state.

$$\text{Curve } a\text{:} \quad T_a(t) = \frac{P_{\rm cons} + GT_{\rm s}}{G} + \frac{\varepsilon_{\rm e} P_0}{C{\rm i}w + G}\exp({\rm i}wt) + c_1 \exp\Big(-\frac{G}{C}t\Big), \tag{13}$$

$$\text{Curve } b\text{:} \quad T_b(t) = \frac{P_{\rm cons} + GT_{\rm s} + b_{p_{\rm v}}}{G - k_{p_{\rm v}}} + \frac{\varepsilon_{\rm e} P_0}{C{\rm i}w + G - k_{p_{\rm v}}}\exp({\rm i}wt) + c_1' \exp\Big(-\frac{G - k_{p_{\rm v}}}{C}t\Big), \tag{14}$$

$$\text{Curve } c\text{:} \quad T_c(t) = \frac{P_{\rm cons} + GT_{\rm s}}{G} + \frac{\varepsilon_{\rm e} P_0}{C{\rm i}w + G}\exp[{\rm i}w\Big(t - t_{\rm f}\Big)] + c_1 \exp\Big[-\frac{G}{C}(t - t_{\rm f})\Big]. \tag{15}$$

It can be found in Fig. 5 that, at $t = 0$, the values of curves a and b are the same; at $t = t_{\rm int}$, the values of curves b and c are the same; since there is no modulation device in microbolometers, thus when $w = 0$, combining Eqs. (13), (14) and (15), we have:

$$T_b(0) = \frac{P_{\rm cons} + GT_{\rm s} + b_{p_{\rm v}}}{G - k_{p_{\rm v}}} + \frac{\varepsilon_{\rm e} P_0}{G - k_{p_{\rm v}}} + c_1' = T_a(0) = \frac{P_{\rm cons} + GT_{\rm s}}{G} + \frac{\varepsilon_{\rm e} P_0}{G} + c_1, \tag{16a}$$

$$T_b(t_{\rm int}) = \frac{P_{\rm cons} + GT_{\rm s} + b_{p_{\rm v}}}{G - k_{p_{\rm v}}} + \frac{\varepsilon_{\rm e} P_0}{G - k_{p_{\rm v}}} + c_1' \exp\Big(-\frac{G - k_{p_{\rm v}}}{C}t_{\rm int}\Big) = \frac{P_{\rm cons} + GT_{\rm s}}{G} + \frac{\varepsilon_{\rm e} P_0}{G} + c_1 \exp\Big[-\frac{G}{C}(t_{\rm int} - t_{\rm f})\Big]. \tag{16b}$$

The solution is:

$$c_1 = \frac{\Big[\Big(\dfrac{P_{\rm cons}+GT_{\rm s}}{G} - \dfrac{P_{\rm cons}+GT_{\rm s}+b_{p_{\rm v}}}{G-k_{p_{\rm v}}}\Big) + \Big(\dfrac{\varepsilon_{\rm e}P_0}{G} - \dfrac{\varepsilon_{\rm e}P_0}{G-k_{p_{\rm v}}}\Big)\Big]\Big[\exp\Big(-\dfrac{G-k_{p_{\rm v}}}{C}t_{\rm int}\Big)-1\Big]}{\exp\Big[-\dfrac{G}{C}(t_{\rm int}-t_{\rm f})\Big] - \exp\Big(-\dfrac{G-k_{p_{\rm v}}}{C}t_{\rm int}\Big)},$$

$$c_1' = \frac{\Big[\Big(\dfrac{P_{\rm cons}+GT_{\rm s}}{G} - \dfrac{P_{\rm cons}+GT_{\rm s}+b_{p_{\rm v}}}{G-k_{p_{\rm v}}}\Big) + \Big(\dfrac{\varepsilon_{\rm e}P_0}{G} - \dfrac{\varepsilon_{\rm e}P_0}{G-k_{p_{\rm v}}}\Big)\Big]\Big\{\exp\Big[-\dfrac{G}{C}(t_{\rm int}-t_{\rm f})\Big]-1\Big\}}{\exp\Big[-\dfrac{G}{C}(t_{\rm int}-t_{\rm f})\Big] - \exp\Big(-\dfrac{G-k_{p_{\rm v}}}{C}t_{\rm int}\Big)}. \quad (17)$$

Put c_1 into Eq. (16a):

$$T(0) = T_a(0) = T_b(0) = K_{T(0)} \times P_0 + T_{\rm cons}, \quad (18)$$

where

$$K_{T(0)} = \varepsilon_{\rm e} \times \frac{\exp\Big[-\dfrac{G}{C}(t_{\rm int}-t_{\rm f})\Big] - \dfrac{G}{G-k_{p_{\rm v}}}\exp\Big(-\dfrac{G-k_{p_{\rm v}}}{C}t_{\rm int}\Big) + \dfrac{k_{p_{\rm v}}}{G-k_{p_{\rm v}}}}{G\times\Big\{\exp\Big[-\dfrac{G}{C}(t_{\rm int}-t_{\rm f})\Big] - \exp\Big(-\dfrac{G-k_{p_{\rm v}}}{C}t_{\rm int}\Big)\Big\}}, \quad (19)$$

$$T_{\rm cons} = \frac{P_{\rm cons}+GT_{\rm s}}{G} + \frac{\Big(\dfrac{P_{\rm cons}+GT_{\rm s}}{G} - \dfrac{P_{\rm cons}+GT_{\rm s}+b_{p_{\rm v}}}{G-k_{p_{\rm v}}}\Big)\Big[\exp\Big(-\dfrac{G-k_{p_{\rm v}}}{C}t_{\rm int}\Big)-1\Big]}{\exp\Big[-\dfrac{G}{C}(t_{\rm int}-t_{\rm f})\Big] - \exp\Big(-\dfrac{G-k_{p_{\rm v}}}{C}t_{\rm int}\Big)}. \quad (20)$$

The readout circuit of microbolometer generally performs the integration during the pulse bias period, so in the following we focus on the solution of the curve b.

When $w = 0$, the derivative of curve b is:

$$T_b'(t) = c_1'\frac{k_{p_{\rm v}}-G}{C}\exp\Big(-\frac{G-k_{p_{\rm v}}}{C}{\rm t}\Big), \quad (21)$$

which is a monotonous function.

According to the calculating parameters in Table 1:

$$T_b'(0) = c_1'\frac{k_{p_{\rm v}}-G}{C}, \quad (22)$$

$$T_b'(t_{\rm int}) = T_b'(5\times10^{-5}) = 1.0092c_1'\frac{k_{p_{\rm v}}-G}{C}. \quad (23)$$

Comparing Eqs. (22) and (23), during the heated time of the pixel, the difference of the derivative of $T_b'(0)$ and $T_b'(t_{\rm int})$ is less than 1%, while $T_b'(t_{\rm int})$ is a monotonous function, so in the whole pulse bias period, the biggest change in the derivative of Eq. (21) will not exceed 1%, which means it can be estimated as a straight line:

$$T_b(t) = K_{T(0)} \times P_0 + T_{\rm cons} + c_1'\frac{k_{p_{\rm v}}-G}{C}t \quad (0 \le t \le t_{\rm int}). \quad (24)$$

The typical expression of $R(T)$ in Ref. [15] is $R(T) = R(T_{\rm s})\exp[\alpha(T-T_{\rm s})]$, then, the mathematical model of the resistance of the pixel is:

$$R(t) = R(T_{\rm s})\exp\Big\{\alpha\Big[\Big(K_{T(0)}P_0 + T_{\rm cons} + c_1'\frac{k_{p_{\rm v}}-G}{C}t\Big) - T_{\rm s}\Big]\Big\} \quad (0 \le t \le t_{\rm int}). \quad (25)$$

Figure 6 is the structure of the readout circuit of the French-made ULIS 320 × 240 uncooled FPA detector which adopts the CTIA input circuit structure and pulsed voltage bias mode. The bias resistance shares the same material with the sensitive element resistance. Rb does not absorb the outside IR radiation; the current into the integration capacitance is the difference between the currents through Rb and through the sensitive element. During the integration time, the pixel switch $K_{\rm p}$ is closed, the currents through the pixel $i_{\rm p}(t)$ and through Rb are:

$$i_{\rm p}(t) = (V_{\rm FID} - V_{\rm TH_FID})/R(t), \quad (26)$$

$$i_{\rm b} = (V_{\rm EBASAGE} - V_{\rm TH_EBASAGE})/Rb, \quad (27)$$

where $V_{\rm FID}$ represents the FET gate voltage; $V_{\rm TH_FID}$, $V_{\rm TH_EBASAGE}$ represent FET threshold voltages; $(V_{\rm FID} - V_{\rm TH_FID})$ is the voltage applied to the pixel; $V_{\rm EBASAGE}$ is the bias voltage applied to one side of Rb; $R(t)$ is the value of the pixel resistance. The current directions of $i_{\rm p}(t)$ and $i_{\rm b}$ are shown in Fig. 6.

Thus, the current into the integration capacitance $(i_{\rm int}(t))$ is:[16]

$$i_{\rm int}(t) = i_{\rm b} - i_{\rm p}(t) = (V_{\rm EBASAGE} - V_{\rm TH_EBASAGE})/Rb - (V_{\rm FID} - V_{\rm TH_FID})t/R(t). \tag{28}$$

The sampling voltage ($V_{\rm samp}$) acquired by the sampling capacitance after the integration time is:

$$V_{\rm samp} = V_{\rm cons} - \big(1/C_{\rm int}\big) \int_0^{t_{\rm int}} \Big[(V_{\rm EBASAGE} - V_{\rm TH_EBASAGE})/Rb - (V_{\rm FID} - V_{\rm TH_FID})/R(t)\Big] {\rm d}t, \tag{29}$$

where $V_{\rm cons}$ is the voltage on the positive side of the reverse amplifier in the CTIA input circuit; $t_{\rm int}$ is the integration time.

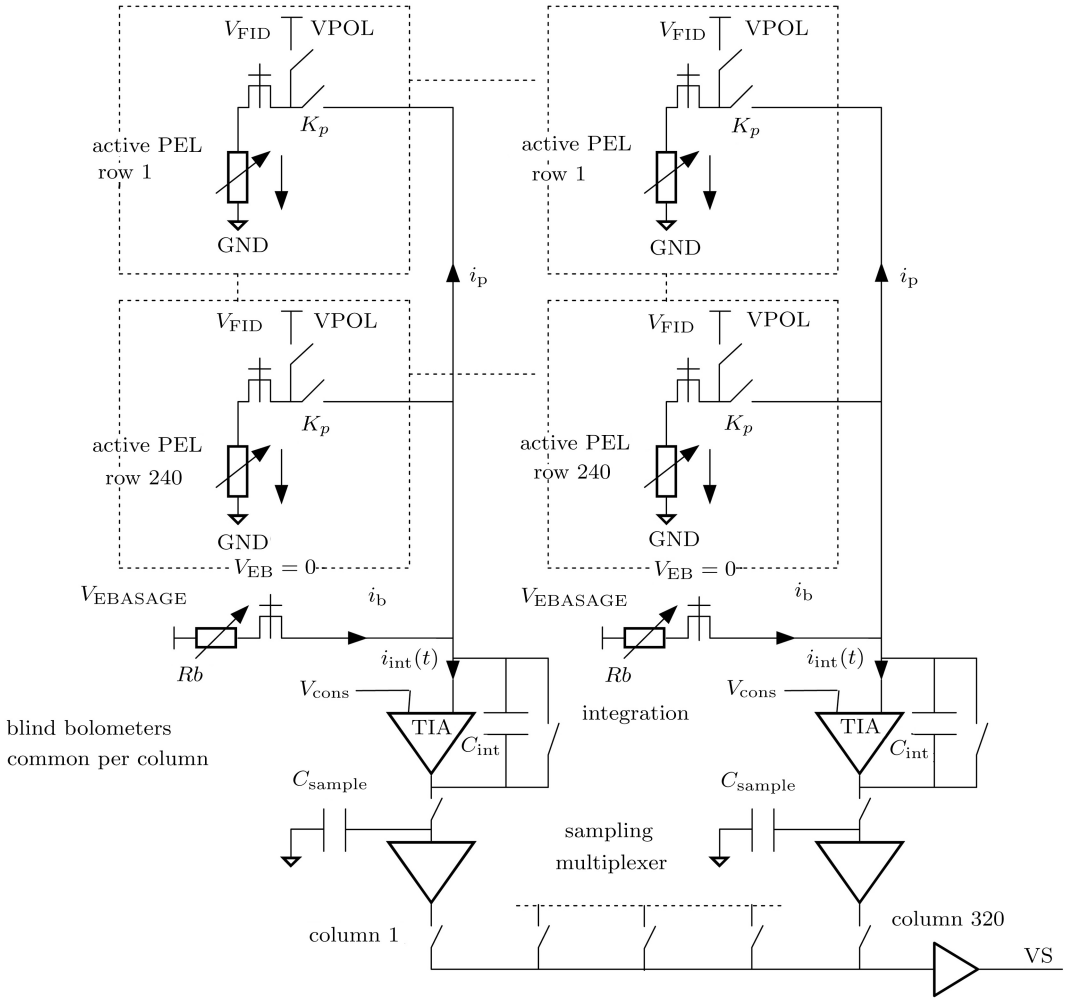


Fig. 6. Schematic structure of the readout circuit of the 320 × 240 uncooled FPA detector made by ULIS.

According to Ref. [17]:

$$E = (1/4)K\sigma T^4 \times (2a/f')^2, \tag{30}$$

$$P_0 = E \times A_{\rm s}. \tag{31}$$

Combining Eqs. (25), (29), (30), and (31):

$$V_{\rm samp} = V_{\rm cons} - \frac{1}{C_{\rm int}} \Big\{ \big[(V_{\rm EBASAGE} - V_{\rm TH_EBASAGE})t_{\rm int}/Rb\big] + \frac{(V_{\rm FID} - V_{\rm TH_FID})C}{R(T_{\rm s})\alpha(k_{\rm pv} - G)c_1'} \times \Big\{ \exp\Big[-\alpha\Big(K_{T(0)}P_0 + T_{\rm cons} - T_{\rm s} + c_1' \frac{k_{p_{\rm v}} - G}{C} t_{\rm int}\Big)\Big] - \exp\big[-\alpha(K_{T(0)}P_0 + T_{\rm cons} - T_{\rm s})\big] \Big\} \Big\}, \tag{32}$$

where $P_0 = (1/4)A_{\rm s}K\sigma T^4 \times (2a/f')^2 \times \beta_{\rm p}^2/(\beta_p - \beta)^2$.

If the temperature T of the IR target is used as the variable, the mathematical response model of the uncooled IRFPA detector is:

$$V_{\rm samp}(T) = V_{\rm cons} - \frac{1}{C_{\rm int}}\Big\{l_{\rm P01} + m_{\rm p01} \times \frac{\exp(n'_{\rm p01}T^4 + n'_{\rm p02}) - \exp(n_{\rm p01}T^4 + n_{\rm p02})}{c_2 + c'_2T^4}\Big\}, \tag{33}$$

where

$$l_{\rm p01} = (V_{\rm EBASAGE} - V_{\rm TH_EBASAGE}) \times t_{\rm int}/Rb, \qquad m_{\rm p01} = (V_{\rm FID} - V_{\rm TH_FID})C/R(T_{\rm s})\alpha(k_{\rm pv} - G),$$
$$n_{\rm p01} = -(1/4)\alpha K_{T(0)}A_{\rm s}K\sigma \times (2a/f')^2 \times \beta_{\rm p}^2/(\beta_{\rm p} - \beta)^2, \qquad n_{\rm p02} = -\alpha(T_{\rm cons} - T_{\rm s}),$$
$$n'_{\rm p01} = -(1/4)\alpha K_{T(0)}A_{\rm s}K\sigma \times (2a/f')^2 \times \beta_{\rm p}^2/(\beta_{\rm p} - \beta)^2 - \alpha c'_2\frac{k_{p_{\rm v}} - G}{C}t_{\rm int},$$
$$n'_{\rm p02} = -\alpha(T_{\rm cons} - T_{\rm s}) - \alpha c_2\frac{k_{p_{\rm v}} - G}{C}t_{\rm int}.$$

4. Model verification

The mathematical response model of the uncooled IRFPA detector is conducted on the basis of the ULIS made 320×240 microbolometer, so the model established in Section 3 will still be verified by analysing this detector. The 7-MHz and 9-MHz master clocks (MC) are used separately to drive this detector, and then we calculate the unknown parameters in Eq. (33), which does a great help to complete the whole model. Table 4 is the comparison table between the sampling voltage values calculated by the model and the tested values. The test condition is: F# of infrared lens: 1.0; f of infrared lens: 50 mm; integration time of IRFPA: 35.56 μs; $V_{\rm FID}$ of IRFPA: 1.4661 V; $V_{\rm EBASAGE}$ of IRFPA: 3.028 V; frame time: 40 ms; temperature surrounding IRFPA: 27 °C.

Table 4. The comparison table of the theoretical sampling voltage value and the tested value.

target tempreture/K	9-MHz MC		7-MHz MC	
	theoretical value/V	tested value/V	theoretical value/V	tested value/V
300	1.249	1.249	0.671	0.671
302	1.262	1.262	0.687	0.687
304	1.275	1.275	0.704	0.704
306	1.288	1.288	0.721	0.721
308	1.301	1.302	0.739	0.740
310	1.315	1.316	0.756	0.757
312	1.329	1.330	0.774	0.775
314	1.344	1.345	0.793	0.794
316	1.359	1.360	0.812	0.813
318	1.373	1.374	0.831	0.832
320	1.389	1.390	0.851	0.852
322	1.404	1.405	0.871	0.872
324	1.420	1.421	0.891	0.893
326	1.436	1.438	0.912	0.914
328	1.453	1.455	0.934	0.936
330	1.470	1.472	0.955	0.957
332	1.487	1.489	0.978	0.980
334	1.504	1.506	1.000	1.003
336	1.522	1.525	1.023	1.026
338	1.541	1.543	1.047	1.050
340	1.559	1.562	1.071	1.074
342	1.578	1.581	1.095	1.098
344	1.598	1.601	1.120	1.123

Table 4. (continued)

target tempreture/K	9-MHz MC		7-MHz MC	
	theoretical value/V	tested value/V	theoretical value/V	tested value/V
346	1.617	1.621	1.146	1.150
348	1.637	1.641	1.172	1.176
350	1.658	1.662	1.198	1.202
352	1.678	1.682	1.225	1.229
354	1.700	1.704	1.252	1.257
356	1.721	1.726	1.280	1.285
358	1.743	1.748	1.308	1.313
360	1.766	1.771	1.337	1.343
362	1.789	1.794	1.367	1.373
364	1.812	1.817	1.397	1.403
366	1.836	1.841	1.428	1.434
368	1.860	1.865	1.458	1.465
370	1.885	1.890	1.491	1.498
372	1.910	1.916	1.523	1.530
374	1.935	1.942	1.556	1.564
376	1.961	1.968	1.589	1.597
378	1.987	1.994	1.623	1.632
380	2.014	2.021	1.658	1.667
382	2.042	2.050	1.694	1.703
384	2.070	2.078	1.730	1.740
386	2.098	2.106	1.766	1.776
388	2.127	2.136	1.804	1.814
389	2.142	2.151	1.823	1.833

From the table, it can be concluded that, when the target temperature is in the range of 300 K to 389 K, the maximum difference between the tested data and the theoretical values is less than 10 mV, so in the dynamic range of 90 K, the difference between the target temperature and the tested temperature calculated by the model is 1 K. For the commonly used dynamic range of 30 K, the difference is less than 2 mV using this model, the biggest temperature difference is 0.2 K. Thus, in the common use of IRFPA detector, this model can perform well to describe the actual detector response.

5. Conclusion

In this paper, we researched the theory of microbolometer, and formulated the heat balance equation under the pulsed voltage bias condition, and finally established the mathematical response model of microbolometer. The experimental data show that this model gives a maximum difference of 0.2 K between the tested data and the model data in the temperature dynamic range of 30 K, and 1 K in the temperature dynamic range of 100 K, which proves that this model reflects the real response of microbolometer effectively.

References

[1] Nicholas G, Kedar K and Wanli C 2008 *Appl. Opt.* **47** A7

[2] Cen L B, Shen B, Qin Z X and Zhang G Y 2009 *Chin. Phys.* B **18** 5366

[3] De A L A L, Deep G S, Lima A M N, Khrebtov I A, Malyarov V G and Neff H 2004 *Appl. Phys. Lett.* **85** 3605

[4] Luiz A L D A, Gurdip S D A M N L and Helmut N 2002 *Opt. Eng.* **41** 2582

[5] Wood A 1996 *Semiconduct. Semimet.* **47** 45

[6] Kruse P W, Mc G L D and McQuistan B R 1962 *Elenments of Infrared Technology* (New York: John Wiley)

[7] Jiang S E, Zheng Z J, Cheng J X and Sun K X 2000 *Acta Phys. Sin.* **49** 1507 (in Chinese)

[8] Yu X Y, Ding X, Li Z, Xu J J and Zhang G Y 2002 *Acta Phys. Sin.* **51** 1307 (in Chinese)

[9] Zhang D M 2001 *Acta Phys. Sin.* **50** 914 (in Chinese)

[10] Liu D, Wang F, Huang Q X, Yan J H, Chi Y and Cen K F 2008 *Chin. Phys.* B **17** 1312

[11] Guan Z Q, Abe Y, Jiang D H, Lin H, Yamazaki Y and Wu C X 2004 *Chin. Phys.* **13** 105

[12] Appel J W and Galeazzi M 2006 *Infrared Phys. Technol.* **562** 272

[13] Franz K, Franz K, Artur J and Johannes S 2004 *Infrared Phys. Technol.* **115** 308

[14] Li Y W 2003 *Research on Uncooled Staring IR Imaging Technology* (Wuhan: Huazhong University of Science and Technology Press) (in Chinese)

[15] Chang B K and Cai Y 2006 *Infrared Imaging Arrays and Systems* (Beijing: Science Press) (in Chinese)

[16] Michael A Dem'yanenko 2007 *Proceedings of SPIE* **6542** 654222-1

[17] Li X T 1997 *Geometrical Optics and Optical Design* (Hangzhou: Zhejiang University Press) (in Chinese)